



Different Contrast Mechanisms in SEM Imaging of Graphene

Application Note

Jining Xie and James P. Spallas
Agilent Technologies

Introduction

Modern scanning electron microscopes (SEMs) all utilize digital scan controls, digital signal acquisition and processing of gray-scale digital images. In a working digital SEM, high energy electrons are focused into a fine beam which rasters across the surface of a specimen pixel by pixel in incremental steps. A complex beam/specimen interaction at each pixel generates a variety of signals which are detected and exhibited on a display unit scanning in synchronism with the beam scan on the specimen. When the focused beam is addressed to a certain point on the specimen, the signal intensity is measured by a detector integrating for the dwelling time, and represented as the brightness of the pixel in a digital image. The intensity is typically digitized into a range of 8 bits which gives 256 discrete gray levels. Apparently, such gray-level images can be interpreted to reveal some characteristics of the specimen. Since image contrast is always related to some properties of the specimen, understanding the concept of contrast and its numerical meaning is of great importance in scanning electron microscopy. Various contrast mechanisms have been developed throughout the history of SEM. Common types include topographic contrast and compositional/elemental

contrast which apply for virtually all specimens and provide the foundation of SEM image formation. Additionally, some special contrast mechanisms, such as electric field contrast, magnetic contrast, and crystallographic contrast, exist for certain types of materials and are related closely to their special properties.

As a powerful technique, SEM has been extensively used for imaging new materials, especially at micro- and nanoscales. Graphene consisting of a monolayer of sp^2 bonded carbon atoms is a relatively new member of the carbon family. But owing to its unique structure, exceptional electrical, optical and mechanical properties, graphene is a rapidly rising star on the horizon of materials science and condensed matter physics [1]. Since its discovery, optical microscopy, atomic force microscopy, transmission electron microscopy and micro-Raman spectroscopy have been widely employed to investigate its optical properties, determine its thickness, resolve its atomic arrangement, and detect its film quality, respectively. In addition to these imaging techniques, there is a growing emphasis of using SEM as a rapid, non-invasive and effective manner for imaging the morphologies of graphene films. Particularly, many



Agilent Technologies

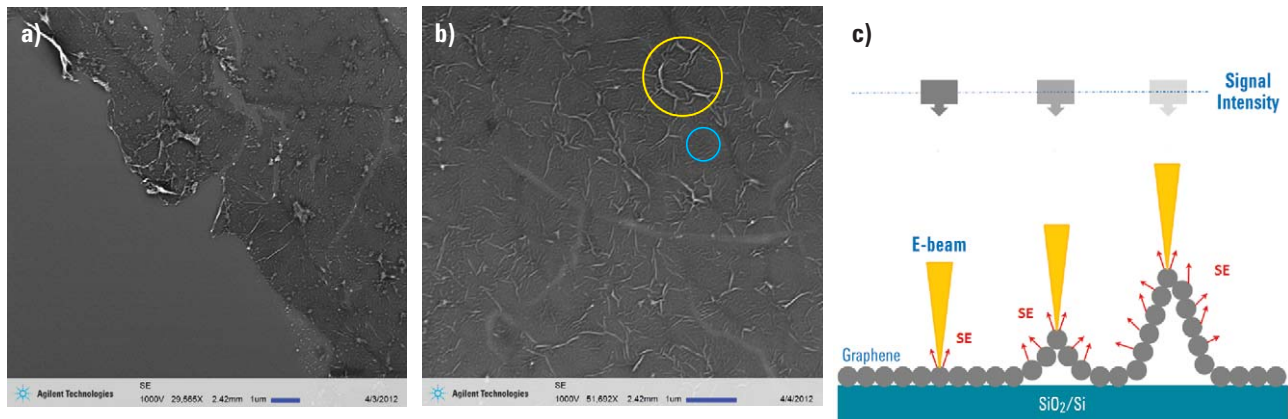


Figure 1. a) A SEM micrograph showing the edge of a transferred graphene sheet on the SiO₂/Si substrate; b) a highly corrugated structure with small and big wrinkles, indicated as the blue circle and yellow circle, respectively; c) a schematic depicting the roughness contrast for a corrugated graphene sheet on the SiO₂/Si substrate.

electronic applications require uniform and defect free graphene in large area. SEM has the advantages in detecting impurities, ruptures, folds, voids and discontinuities of synthesized or transferred graphene on a variety of substrates. However, SEM imaging of graphene is difficult mainly because of the following reasons. First, imaging an atomic-thick graphene layer is quite challenging due to the resolution limitation of SEMs. Secondly, the ultra-thin graphene layer is “transparent” to high energy electron beams. Hence SEM images easily display the morphologies of the substrate beneath the graphene, not the graphene itself. Furthermore, sometimes graphene films are too smooth to generate sufficient contrasts in SEM imaging. Although such a weak contrast can be enhanced by digital imaging processing, this process also magnifies the noise level simultaneously and may lead to an unacceptable image quality.

Imaging graphene with a low beam voltage field emission scanning electron microscope (LV FE-SEM) is very promising because of its unique combination of high resolutions, a small beam/specimen interaction volume, enhanced contrasts and the capability of revealing more surface details. The object of this work is to discuss possible mechanisms of several contrasts observed in

graphene imaging by using an Agilent 8500 compact FE-SEM. With an innovative design of a miniature electrostatic electron beam column, Agilent 8500 can achieve sub 10nm resolution working at low beam voltages which makes it a good imaging tool for graphene films. The beam voltage was set as 1kV throughout this imaging work. Three typical contrasts in SEM imaging of graphene including surface roughness contrast, edge contrast, and thickness contrast will be discussed in the following.

Surface Roughness Contrast

A good quality graphene film should be smooth, continuous and free of impurities. Obtaining a “perfect” monolayer single-crystal graphene domain in large area is always the goal for all synthesis methods and a number of successes have been demonstrated. In many cases, synthesized graphene sheets are required to transfer to different substrates for versatile applications. Unfortunately, this transfer process usually produces many defects such as wrinkles, ruptures, folds and voids, or even introduces impurities. Detecting such defects on transferred graphene sheets is needed for quality control purposes. Low voltage FESEM provides a good solution for this demand.

Figure 1a shows the morphology of a transferred graphene sheet on a silicon substrate covered with ~290 nm SiO₂. The edge of a ruptured sheet was selected for viewing both graphene and the SiO₂ surface. It is obvious that, compared with the smooth SiO₂ surface, the graphene sheet has a much rougher surface with some impurities and cracks. This roughness contrast can be explained as the topographic contrast which is the most frequent application of the SEM. The topographic contrast has a complex origin and arises from the dependence of the number and trajectories of electrons (SE and BSE) on the angle of incidence between the beam and the specimen surface [2]. In a higher magnification image, Figure 1b, a highly corrugated structure can be seen clearly. Two types of wrinkles with different contrasts were observed, as indicated in the areas enclosed by blue and yellow circles. The higher contrast in the yellow circle area represents a higher roughness than features in the blue circle area. At this situation, it is reasonable to relate the signal intensity with the height of the feature. As depicted in Figure 1c, the roughness contrast of a graphene sheet comes from different numbers of SE detected. For rougher features, more SE will escape from the graphene surface within the same area resulting in

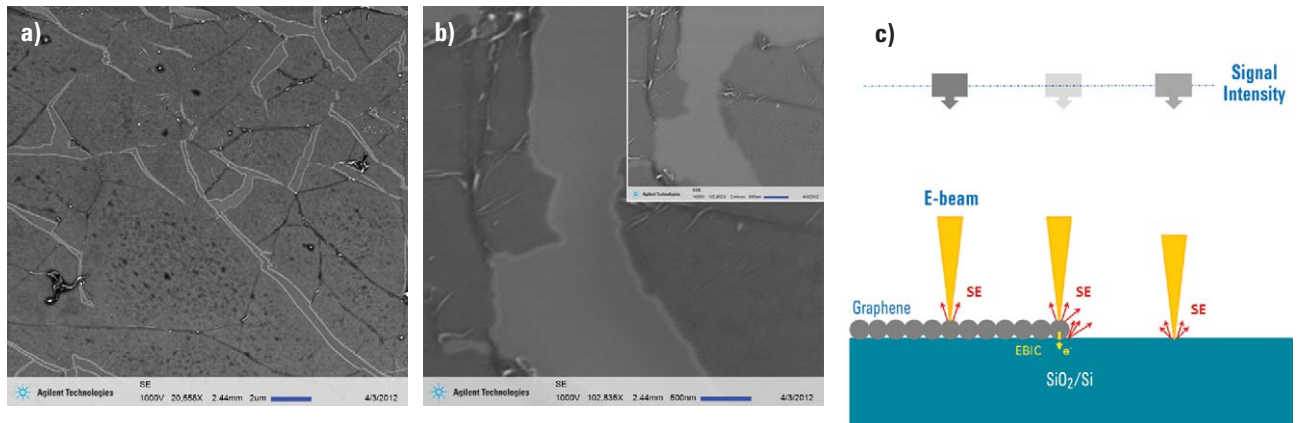


Figure 2. a) A SE image showing bright contour lines around the boundaries of a cracked graphene film. b) A SE image at a higher magnification still exhibits such edge contrast while the BSE image does not (the inset). c) Schematic illustration of the edge contrast caused by both edge effect and EBIC.

higher signal intensity than that from the background (a smoother surface). It is believed that these small and big wrinkles are attributed to the rough metal surface formed in the CVD process and the gap between the graphene layer and the substrate during the transfer process, respectively [3].

Such a rough surface of a continuous graphene film can be imaged well by using an in-lens SE detector while a regular Everhart-Thorney (ET) detector can not reveal the surface details [4]. The in-lens detector collects low-energy secondary electrons efficiently. And the signal detected is relatively enriched in SE1 signals which are more surface sensitive. Because of its ultrathin thickness, graphene is more sensitive to low energy electrons than high energy electrons. Unlike most regular FE-SEMs, Agilent 8500 uses a four quadrant multi channel plate (MCP) detector located above the specimen for both SE and BSE detections. The MCP detector is well known for good performance in detecting low energy electrons which are sensitive to surface details. As shown in Figure 1, the MCP detector in Agilent 8500 working at low voltages is capable of obtaining detailed surface information from this fine and rough graphene sheet.

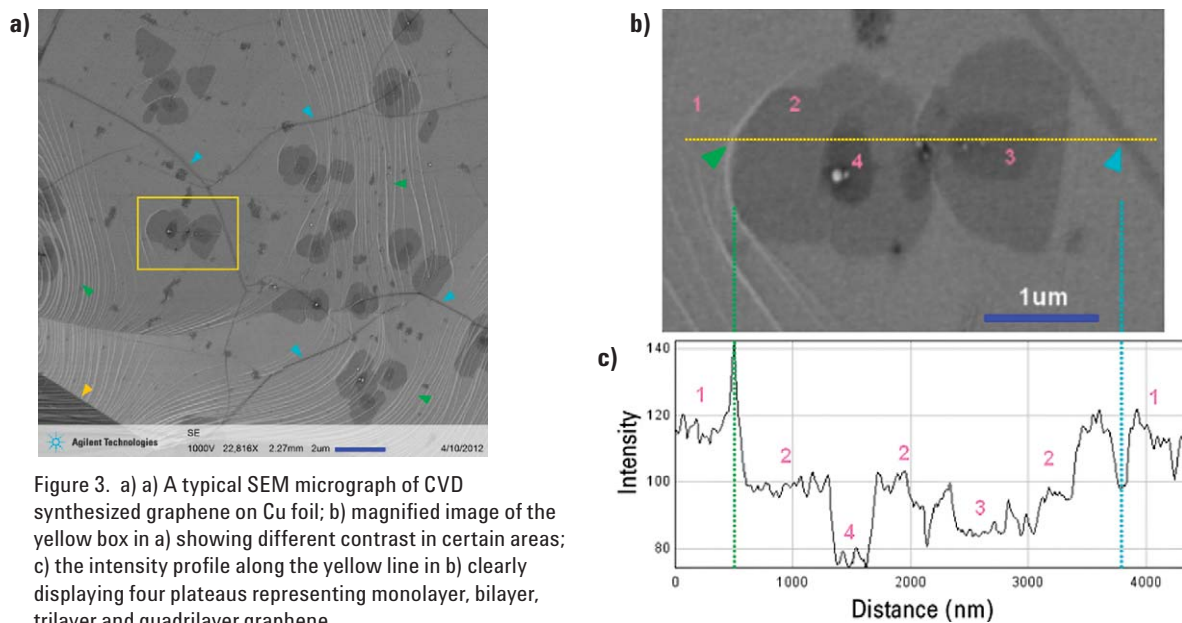
Edge Contrast

Generally, the edge effect can be also explained by the topographic contrast mechanism which is similar to the surface roughness contrast described above. At the edge area, a larger part of the beam/specimen interaction volume will be in the SE escape zone. Therefore more secondary electrons can emit from the side of the edge resulting in higher signal intensity than that from a flat surface. As shown in Figure 2a, the monolayer graphene on a SiO₂/Si substrate exhibits many cracks which were caused in the transfer process. Interestingly, the edges of graphene films display in a high brightness forming obvious white lines along every graphene boundary. It can be seen from Figure 2b that such edge contrast is still obvious even at a high magnification. But this edge contrast disappears in the corresponding BSE image, the inset of Figure 2b.

Considering the ultra-small thickness of a single graphene layer (~ 0.35 nm), it is unlikely that such an imperceptible edge can generate such a remarkable signal contrast. Also, the diameter of the "contour line" (~ 50 nm) is larger than what the edge should be or even much larger than the spot size of the beam used in this work (~ 10 nm). Thus this edge effect of the graphene monolayer on the SiO₂/Si substrate may not be

solely elucidated by the topographic contrast. A similar phenomenon about a much larger diameter observed for single-walled carbon nanotubes on SiO₂ substrates was reported [5, 6]. It seems that the contrast mechanism of electron beam induced current (EBIC) could be used to explain this observed edge effect of graphene films as well.

SiO₂ has a large secondary electron yield, especially at a low beam voltage (e.g. 1 kV). When the emitted secondary electrons outnumber the incident primary electrons, the surface of SiO₂ is positive charged with an electron-depletion due to its poor conductivity. As a result, the increased potential difference will decrease the secondary electron yield. This process will re-establish the neutrality on the surface. When covered by a graphene layer, the secondary electron yield of SiO₂ will be affected and part of the detected SE signals will come from the graphene surface. A possible mechanism of the graphene-covered area showing a darker color will be discussed in the next section. Considering the edge of the graphene layer where SiO₂ is exposed but also contacts with graphene, the following process may occur in sequence: 1) the surface of SiO₂ is positive charged due to its high SE yield; 2) this potential difference induces electrons flowing from graphene to SiO₂ to replenish



electrons in the vicinity; 4) thus the high SE yield of the SiO₂ surface is recovered resulting in a high brightness. Figure 2c illustrates the edge contrast caused by both edge effect and EBIC. In the SE image, the bright edge line with a diameter larger than the spot size of the electron beam actually reflects the EBIC range from the SiO₂ surface. This edge contrast is prominent in low beam voltage imaging because the low energy incident electrons do not penetrate through the thin SiO₂ layer and reach the Si substrate, hence only the graphene layer supplies the EBIC. The disappearance of the bright contour lines in the BSE image could be attributed to the higher energy of BSEs and their straight trajectories.

Thickness Contrast

Graphene films may contain a single layer to a few layers. Chemical vapor deposition (CVD) offers significant advantages over the mechanical exfoliation, particularly when pursuing a large area production. The as grown graphene films synthesized by CVD usually contain multi-layer domains [7]. Optical microscopy has been commonly used to test the uniformity of synthesized

graphene films on the SiO₂ surface and even is able to identify the number of graphene layers based on an observed contrast changing. A change of color contrast in optical images indicates a variation of the graphene film thickness because the light interference on the SiO₂ layer is modulated by the graphene layers [8, 9]. This optical microscopy method is effective and also gives a wide field of view. However, this it is limited to identification of graphene layers on ~300 nm SiO₂ and it has a low spatial resolution due to the diffraction limits of light. The observed thickness contrast in SEM imaging of graphene films may offer an alternative means for the same purpose.

To test the uniformity of graphene films, a CVD derived graphene on a copper foil was used for LV FE-SEM imaging. Figure 3a is a typical SEM micrograph displaying some features of the Cu foil and the graphene film. In addition to Cu grain boundaries (indicated as the orange arrow head), some narrow, white lines (indicated as green arrow heads) represent the typical Cu terracing consisting of many steps. As the CVD growth mechanism of graphene layers, graphene grows from a

nucleus, crosses Cu steps and grain boundaries, and covers the whole surface. Multiple graphene layers grown from different nuclei randomly can coalesce to form multilayer graphene [10]. As shown in Figure 3a, the background color is assigned to a graphene monolayer covering the whole Cu surface. Those narrow, dark lines are graphene “wrinkles”, which is a signature feature of CVD grown graphene layers on Cu foils. They are associated with the difference of thermal expansion coefficients between graphene and Cu during the CVD process. The wrinkles crossing the Cu steps and boundaries imply the continuity of the graphene film. Some flakes with darker colors indicate graphene with multiple layers. As shown in Figure 3b, a magnified image of the yellow box area in Figure 3a, area 1, 2, 3 and 4 with decreasing brightness can be attributed to monolayer, bilayer, trilayer, and quadrilayer graphene films, respectively. Similar SEM results with identification of the layer numbers by SEM and confirmation by Raman spectroscopy have been reported [11]. The SE intensity profile along the yellow line extracted from Figure 3b is shown in Figure 3c. Obviously, area 1, 2, 3 and 4 can

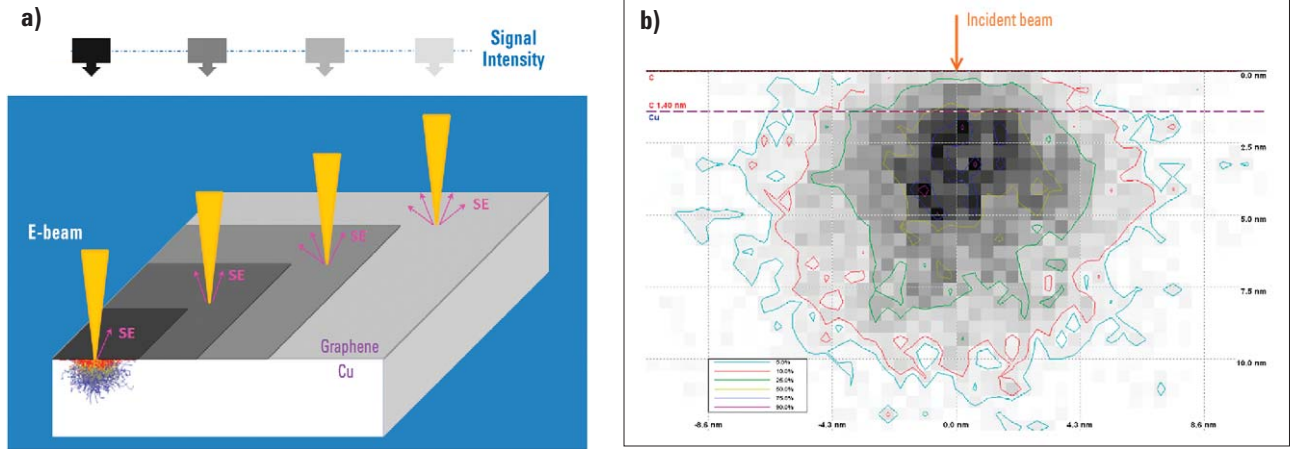


Figure 4. a) Schematic diagram depicting different numbers of SE escaped from graphene films with different numbers resulting in signal contrast; b) Monte Carlo simulation result illustrating the energy distribution by position for a 1kV beam interacting with a quadrilayer graphene on the Cu substrate.

be identified based on their signal intensities. Also, a strong peak (the green arrow head) and a trough (the cyan arrow head) correspond to a Cu step edge and a graphene wrinkle, respectively. This result implies that the signal intensities coming from graphene depend upon the numbers of layers. And the intensity profiles may also suggest a feasible method to quantitatively identify the number of graphene layers based on the values of the intensities obtained from SEM images.

The schematic shown in Figure 4a illustrates the observed contrasts related to various thicknesses of graphene. In order to build up the relationship between signal intensities and graphene thickness, it is necessary to explore the possible mechanism which can explain the thickness contrast of graphene films observed in SEM images. One mechanism reported recently is based on the work function change with the number of graphene layers [12]. It was reported that the work function of graphene increases with the number of layers: from ~4.3eV for monolayer to ~4.6eV for quadrilayer, but it saturates for more layers [13]. The SE yield δ is related to the work function according to the following formula [14]:

$$\frac{\partial \delta}{\partial E_k} = \frac{F' E_k}{(E_k + \phi)} \quad (1)$$

where ϕ is the work function of graphene, E_k is the SE's energy, and F' is a normalization factor. Formula 1 indicates that the SE yield is inversely proportional to the work function of the material from where secondary electrons are generated. Hence a graphene monolayer with a lower work function produces more secondary electrons than a few layer graphene. However, the work function ϕ is small comparing with the energy E_k . Such a small change of work function unlikely causes the observed grey-scale contrasts. Also, the SE yield for such a thin graphene layer is a fraction of the total SE yield. This hypothesized contrast mechanism disappears at this thickness where SE yield from the graphene dominates. Further, this mechanism cannot explain the discrete contrasts discernable for graphene films up to 10 layers [15], because the work function of graphene doesn't change with the layer numbers larger than 4. Therefore, this mechanism alone can not count for the thickness contrast.

The work function mechanism only considers the secondary electrons generated from graphene and ignores the effect of the substrate beneath.

We believe that the substrate has to be counted because the graphene film is so thin that the incident electrons will penetrate the graphene and interact with the substrate. The energy distribution by position for a 1kV beam with 10nm spot size on quadrilayer graphene (~1.4 nm thick)/ Cu substrate is shown in Figure 4b. This result was obtained by the CASINO Monte Carlo simulation [16]. It can be seen that, under the current condition in this study, a significant part of the beam/specimen interaction volume is located inside the Cu substrate. As a consequence, the secondary electrons emitted from the Cu substrate can not be ignored, and actually contribute for the detected signal instead. Recently, Auger electron spectroscopy was demonstrated for a quantitative determination of the thickness of graphene layers up to 6 layers [17]. It was found that the pronounced contrast in Auger maps could be explained in term of the attenuation of low-energy electrons in graphene layers. The energy relaxation of electrons modulates the intensity with varying thickness of graphene layers. Prompted by this observation, the contrast in SEM imaging was explored for graphene films covering SiO₂ surface and came up with a contrast mechanism caused by a

similar SE attenuation combined with differential surface charging and EBIC [18]. In the case of this study, neither voltage contrast nor EBIC needs to be counted because of the conducting Cu substrate. Thus, it is expected that the thickness contrast may be primarily induced by the attenuation of secondary electrons emitted from the Cu substrate by the graphene layers. As illustrated in Figure 5a, a higher number of graphene layers result in lower signal intensity. This hypothesis is based on several assumptions: 1) the interaction volume difference in Cu beneath graphene with a few layers is negligible; 2) there is no inelastic attenuation in the outermost graphene layer; 3) no diffraction effect from the crystalline graphene needs to be considered. By adopting the formula for Auger electron attenuation in graphene layers, we can simplify the intensity of detected SE signals after attenuation as:

$$I_N = Ae^{-N \cdot \frac{d_0}{\lambda}} + B \quad (2)$$

where I_N , d_0 and λ are the SE intensity detected after attenuation by N layers of graphene, the thickness of graphene monolayer and the electron inelastic mean free path, respectively. A and B are fitting parameters which are introduced to offset the intensity adjustment by the digital image processing. Formula 2 implies that the detected signal intensity should decrease exponentially with

the increasing number of graphene layers. By using the intensity values extracted from Figure 3c, we plot the curve of intensity vs. number of layers, as shown in Figure 5b. For such graphene layers observed in this sample, the curve matches well with an exponential formula, indicative of the correctness of the hypothesis.

In addition to the capability of differentiating graphene layers with different thicknesses based on the observed contrasts, SEM imaging also holds the potential for quantitative determination of the number of graphene layers. It has been demonstrated that the properties of graphene films depend strongly on the layer numbers. Raman spectroscopy is commonly used for layer number determination due to its high reliability. But it has a major drawback that the laser irradiation may cause a structural degradation of the graphene [19]. SEM could be employed as an alternative characterization technique which is complementary to optical microscopy and Raman spectroscopy for this purpose. To put it into a practical use, calibration with a standard sample is prerequisite. Then an unknown graphene sample needs to be characterized at the exactly same imaging condition. Special carefulness should be taken to avoid any unnecessary contrast and brightness adjustments. Thus the intensity values extracted from

SEM images can be directly used to determine the number of graphene layers.

Other Possible Contrasts

There are several other contrasts possibly involved in SEM imaging of graphene. One of them is the substrate charging contrast which can be observed when imaging graphene films on insulating substrates. Even for a low voltage electron beam, interaction of the beam with the insulating substrate is significant. If the SE yield is less than 1, a negative potential will be established because of the accumulation of charges on the substrate surface. Consequently, this negative potential will repel incident electrons and the increased signal can not give any morphology information. This unwanted contrast can be controlled by lowering the beam voltage or decreasing the beam dwelling time at each pixel. Another possible contrast mechanism is the elemental contrast in BSE imaging. For non-uniform graphene film on various substrates, it is possible to obtain BSE images showing the compositional contrast due to the difference in BSE yields between carbon and other elements. But actually, it is not as easy as it appears. Such an elemental contrast based on different elements is obvious in high voltage BSE imaging. Unfortunately thin graphene films might be “transparent” for a high

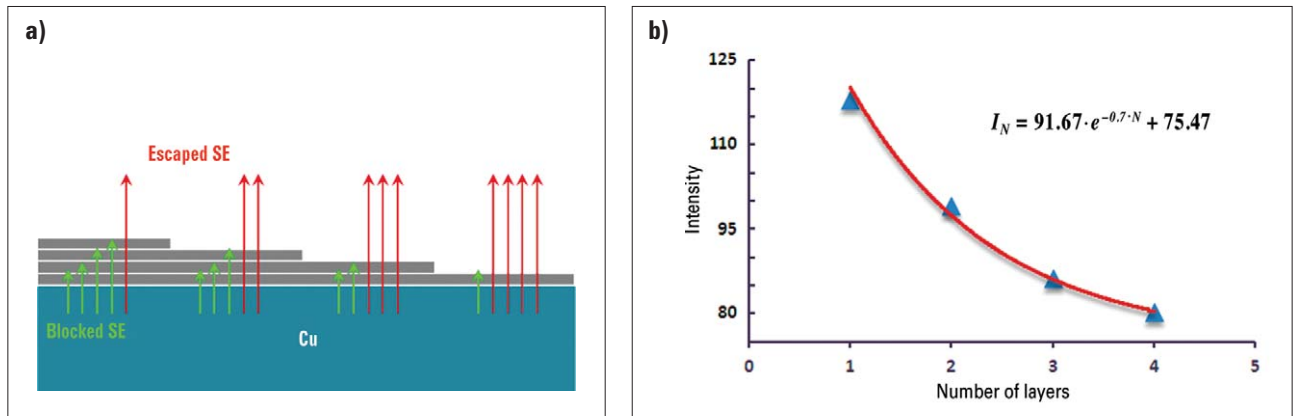


Figure 5. a) schematic depicts the secondary electrons emitted from Cu substrate are attenuated by graphene layers; b) plot of intensity vs. number of graphene layers.

energy electron beam because of its high penetration depth. On the other hand, the composition contrast for low voltage BSE imaging is very weak and may not be able to provide any useful information.

An interesting phenomenon of contrast reversal in graphene monolayer on SiO₂ surface has been observed [18]. At that particular imaging condition, the contrast of graphene reversed at low beam voltages compared with the substrate. This could be caused by differential surface charging due to EBIC. In this work, a similar contrast reversal was observed at the imaging condition employed. However, it is believed that both the substrate charging accumulation and the “auto contrast” adjustment based on the exceptionally bright edge lines are responsible for this phenomenon.

Summary

Owing to its high resolution, high contrast and high surface sensitivity, Low voltage FE-SEM is suitable for graphene imaging. Imaging at 1kV was carried out in this study to reveal surface morphologies of different graphene films. Typical contrasts observed in this work include surface roughness contrast, edge contrast and thickness contrast. Attempts were also made to discuss the possible contrast mechanisms involved in graphene imaging such as topographic contrast, electron beam induced current, and secondary electron attenuation. It was demonstrated that low voltage FE-SEM is able to not only reveal the surface details of graphene films, but also differentiate their different thicknesses.

Acknowledgement

The authors thank Dr. Ying Feng and Prof. Ke Chen at Temple University for kindly providing all graphene samples for this application note as well as valuable discussions.

References

- [1] A.K. Geim and K.S. Novoselov, *Nature Materials* 6, 183 (2007).
- [2] J. Goldstein, D. Newbury, D. Joy, C. Lyman, P. Echlin, E. Lifshin, L. Sawyer and J. Michael, *Scanning Electron Microscopy and X-Ray Microanalysis*, 3rd Edition, Springer (2003).
- [3] X. Liang, B.A. Sperling, I. Calizo, G. Cheng, C.A. Hacker, Q. Zhang, Y. Obeng, K. Yan, H. Peng, Q. Li, X. Zhu, H. Yuan, A.R. Hight Walker, Z. Liu, L. Peng and C.A. Richter, *ACS Nano* 5, 9144 (2011).
- [4] A. Ismach, C. Druzgalski, S. Penwell, A. Schwartzberg, M. Zheng, A. Javey, J. Bokor and Y. Zhang, *Nano Letters* 10, 1542 (2010).
- [5] T. Brintlinger, Y.-F. Chen, T. Dürkop, E. Cobas, M.S. Fuhrer, J.D. Barry and J. Meingalis, *Applied Physics Letters* 81, 2454 (2002).
- [6] Y. Homma, S. Suzuki, Y. Kobayashi, M. Nagase and D. Takagi, *Applied Physics Letters* 84, 1750 (2004).
- [7] I. Vlasiouk, M. Regmi, P. Fulvio, S. Dai, P. Datskos, G. Eres and S. Smirnov, *ACS Nano* 5, 6069 (2011).
- [8] P. Blake, E. W. Hill, A.H.C. Neto, K.S. Novoselov, D. Jiang, R. Yang, T.J. Booth, A.K. Geim, *Applied Physics Letters* 91, 063124 (2007).
- [9] A. Reina, X. Jia, J. Ho, D. Nezich, H. Son, V. Bulovic, M.S. Dresselhaus and J. Kong, *Nano Letters* 9, 30 (2009).
- [10] H. Wang, G. Wang, P. Bao, S. Yang, W. Zhu, X. Xie and W.-J. Zhang, *Journal American Chemical Society* 134, 3627 (2012).
- [11] X. Li, W. Cai, J. An, S. Kim, J. Nah, D. Yang, R. Piner, A. Velamakanni, I. Jung, E. Tutuc, S. K. Banerjee, L. Colombo and R.S. Ruoff, *Science* 324, 1312 (2009).
- [12] M.-H. Park, T.-H. Kim and C.-W. Yang, *Surface and Interface Analysis*, doi: 10.1002/sia.4995 (2012).
- [13] H. Hibino, H. Kageshima, M. Kotsugi, F. Maeda, F.Z. Guo and Y. Watanabe, *Physical Review B* 79, 125437 (2010).
- [14] J. Cazaux, *Ultramicroscopy* 110, 242 (2010).
- [15] H. Hiura, H. Miyazaki and K. Tsukagoshi, *Applied Physics Express* 3, 095101 (2010).
- [16] D. Drouin, A.R. Couture, D. Joly, X. Tastet, V. Aimez and R. Gauvin, *Scanning* 29, 92 (2007).
- [17] M. Xu, D. Fujita, J. Gao and N. Hanagata, *ACS Nano* 4, 2937 (2010).
- [18] W. Kochat, A.N. Pal, E.S. Sneha, A. Sampathkumar, A. Gairola, S.A. Chivashankar, S. Raghavan and A. Ghosh, *Journal of Applied Physics* 110, 014315 (2011).
- [19] B. Krauss, T. Lohmann, D.-H. Chae, M. Haluska, K. von Klitzing and J.H. Smet, *Physical Review B* 79, 165428 (2009).

Nanomeasurement Systems from Agilent Technologies

Agilent Technologies, the premier measurement company, offers high-precision, modular nanomeasurement solutions for research, industry, and education. Exceptional worldwide support is provided by experienced application scientists and technical service personnel. Agilent's leading-edge R&D laboratories ensure the continued, timely introduction and optimization of innovative, easy-to-use nanomeasure system technologies.

www.agilent.com/find/nano

Americas

Canada	(877) 894 4414
Latin America	305 269 7500
United States	(800) 829 4444

Asia Pacific

Australia	1 800 629 485
China	800 810 0189
Hong Kong	800 938 693
India	1 800 112 929
Japan	0120 (421) 345
Korea	080 769 0800
Malaysia	1 800 888 848
Singapore	1 800 375 8100
Taiwan	0800 047 866
Thailand	1 800 226 008

Europe & Middle East

Austria	43 (0) 1 360 277 1571
Belgium	32 (0) 2 404 93 40
Denmark	45 70 13 15 15
Finland	358 (0) 10 855 2100
France	0825 010 700*
	*0.125 €/minute
Germany	49 (0) 7031 464 6333
Ireland	1890 924 204
Israel	972-3-9288-504/544
Italy	39 02 92 60 8484
Netherlands	31 (0) 20 547 2111
Spain	34 (91) 631 3300
Sweden	0200-88 22 55
Switzerland	0800 80 53 53
United Kingdom	44 (0) 118 9276201

Other European Countries:

www.agilent.com/find/contactus

Product specifications and descriptions in this document subject to change without notice.

© Agilent Technologies, Inc. 2012
Printed in USA, June 26, 2012
5991-0782EN



Agilent Technologies